

Nonlinear Piezoelectric Shunt Absorber with 2:1 Internal Resonance: Theory and Experiments

Z.A. Shami¹, C. Giraud-Audine², O.Thomas¹

¹Arts et Métiers Institute of Technology, LISPEN, HESAM Université, Lille, France

²Arts et Métiers Institute of Technology, L2EP, HESAM Université, Univ. Lille, Lille, France

Résumé — We present a theoretical and experimental analysis of a new nonlinear semi-passive piezoelectric shunt absorber designed to attenuate the vibrations of an elastic structure under external excitation. This absorber is formed by connecting the elastic structure via a piezoelectric patch to an electrical shunt circuit consisting of a resonant shunt combined in series with a quadratic voltage component. By suitably tuning the shunt's natural frequency, a two-to-one internal resonance occurs, creating a nonlinear antiresonance associated with amplitude saturation that leads to a high attenuation level.

Mots clés — Nonlinear vibration, 2 :1 Internal resonance, Piezoelectric shunt absorber, Saturation phenomenon, Nonlinear antiresonance.

1 Introduction

Piezoelectric shunt absorbers consist of using a piezoelectric transducer to convert the mechanical energy of the host structure into electrical energy in an electronic shunt circuit to dissipate it and/or to counteract the structure's vibrations. Utilizing a dedicated shunt circuit to damp the vibration of a host structure has been firstly proposed in [1] and then many studies have been established to enhance the shunt circuits' performance [2]. Such shunt circuits are passive in their behavior such that the sensing and actuating are served by the piezoelectric transducer. This suggests that they are unconditionally stable in contrary to the active control strategies.

The simplest architectures of electric shunts, as shown in Figure 1 are the resistive shunts (R -shunts) and the resonant shunts (RL -shunts), which are linear in their behavior.

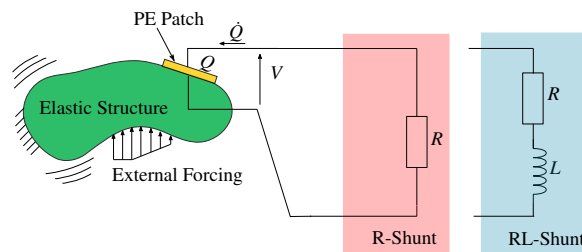


FIGURE 1 – Schematic of the resistive shunts (R -shunts) and resonant shunts (RL -shunts)

The R -shunt attenuates the vibrations by dissipating energy in the form of Joule heat. However, with the RL -shunts, an RLC resonant circuit is coupled to a given mode of the structure to attenuate the vibration level by suitable tuning of the resistor and inductor values. Based on the shunt's behavior, the R -shunts and the RL -shunts are, respectively, the mechanical analogs of the classical Lanchester and Frahm dampers. However, the main advantages in using the electrical analogs rely on the easiness to set and control in many applications.

A nonlinear component can be added to the shunt circuit leading to a nonlinear absorber that exploits some particular features that have no counterpart in the linear theory. Such nonlinear absorbers are firstly analyzed by mechanical dampers and then transposed to the electromechanical analogs. An interesting example is the nonlinear energy sink (NES), proposed in [3]. It consists of attaching to a primary linear structure an essentially nonlinear oscillator into which the vibratory energy is transferred and localized. The extension of the mechanical NES to piezoelectric devices has been theoretically proposed in [4] and

realized with analog circuitry (using multipliers) in [5].

Another feature of the nonlinear absorber is the internal resonance, which occurs when the modal frequencies are commensurable (i.e. $q\omega_q \approx p\omega_j$ with $p, q \in \mathbb{N}^*$). Consequently, a strong coupling between the two corresponding modes occurs, leading to an energy transfer between the modes. A particular type is the two-to-one (2 : 1) internal resonance (i.e., $\omega_2 \approx 2\omega_1$) in which the energy is transferred from the driven mode (near ω_2) to a mode tuned at half this frequency (near ω_1). This leads to two important features [6] : (i) amplitude reduction of the driven mode, where a nonlinear antiresonance replaces the primary resonance, and (ii) a saturation phenomenon that leads to an amplitude of the driven mode independent of the excitation level. Such feature has been exploited to attenuate the vibrations in an active control strategy as done in [7].

The main originality of our work is to use the particular features of a 2 : 1 internal resonance in a semi-passive way using a piezoelectric shunt circuit. In this abstract, we present the theoretical modeling of the absorber with the main analytical and numerical results. In addition, we show some experimental results by connecting the designed absorber to a cantilever beam structure. A complete theoretical and experimental study are illustrated, respectively, in [8] and [9].

2 Theoretical modeling

2.1 Main equations

In this section, a summary of the main equations that govern the electromechanical system is illustrated. We consider an arbitrary elastic structure subjected to an external excitation and connected to a nonlinear shunt circuit via a piezoelectric (PE) patch as shown in Figure 2.

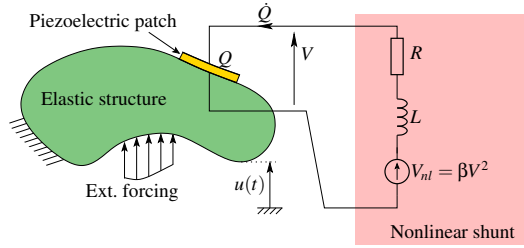


FIGURE 2 – Nonlinear shunt schematic

The displacement vector $\mathbf{u}(\mathbf{x}, t)$ at any point \mathbf{x} of the structure at time t is expanded on a given linear modes $\phi_i(\mathbf{x})$ of the structure in short circuit. One obtains :

$$\mathbf{u}(\mathbf{x}, t) = \phi_i(\mathbf{x})q_i(t), \quad (1)$$

where $q_i(t)$ is the i -th modal coordinate that verifies [8] :

$$\ddot{q}_i + 2\xi_i\hat{\omega}_i\dot{q}_i + \hat{\omega}_i^2q_i + \frac{\theta_i}{m_iC_{pi}}Q = \frac{F_i}{m_i}\cos\Omega t, \quad (2a)$$

$$\ddot{Q} + 2\xi_e\omega_e\dot{Q} + \omega_e^2Q + \frac{\theta_i}{LC_{pi}}q_i + \frac{V_{nl}}{L} = 0. \quad (2b)$$

In the above equations, $Q(t)$ is the electric charge in one of the electrodes of the PE patch and $(m_i, \xi_i, \hat{\omega}_i, F_i, \theta_i)$ are respectively the modal mass, damping, natural frequency in open circuit ($Q = 0$), forcing and piezoelectric coupling coefficient of the i -th mode. C_{pi} is the effective capacitance of the piezoelectric patch [10], and the electrical natural frequency and damping factor are defined by :

$$\omega_e = \frac{1}{\sqrt{LC_{pi}}}, \quad \xi_e = \frac{R}{2}\sqrt{\frac{C_{pi}}{L}}, \quad (3)$$

where (R, L) are, respectively, the resistance and the inductance of the electric circuit. $V_{nl}(t)$ represents the nonlinear voltage source added to the shunt circuit, that is chosen to include quadratic nonlinearities

to activate the 2 : 1 internal resonance. In this study, $V_{nl}(t)$ is taken to be proportional to the square of the voltage $V(t)$ across the piezoelectric patch, by a constant gain β , as shown in Figure 2. One has thus :

$$V_{nl} = \beta V^2, \quad V = \frac{1}{C_{pi}} (Q + \theta_i q_i), \quad (4)$$

where the second equation is the classical constitutive law of the PE patch [8]. We also define the dimensionless electromechanical modal coupling factor (EMMCF) of the i -th mode as :

$$k_i^2 = \frac{\hat{\omega}_i^2 - \check{\omega}_i^2}{\hat{\omega}_i^2} = \frac{\theta_i^2}{\hat{\omega}_i^2 C_{pi} m_i}, \quad (5)$$

with $\check{\omega}_i$ the natural frequency in short circuit ($V = 0$). The system in (2a, b) is linearly coupled through the piezoelectric coupling. To diagonalize the latter system, we further expand it on a basis of two electromechanical modes. This expansion reads :

$$\begin{pmatrix} q_i(t) \\ Q(t) \end{pmatrix} = \begin{pmatrix} \frac{1}{\sqrt{m}} [-\varepsilon x_1(t) + x_2(t)] \\ \frac{1}{\sqrt{L}} [x_1(t) + \varepsilon x_2(t)] \end{pmatrix}. \quad (6)$$

where

$$\varepsilon = \frac{2k_i r_i}{1 - r_i^2 + \sqrt{\Delta}}, \quad (7)$$

with $\Delta = (1 - r_i^2)^2 + 4k_i^2 r_i^2$ and $r_i = \omega_e / \hat{\omega}_i$. Note that ε is small due to the weak piezoelectric coupling ($k_i < 0.2$). The unknowns $x_1(t)$ and $x_2(t)$ are the solution of the following system :

$$\ddot{x}_1 + 2\mu_1 \dot{x}_1 + \omega_1^2 x_1 + \Lambda_1 x_1^2 + \Lambda_2 x_1 x_2 + \Lambda_3 x_2^2 = f_1 \cos \Omega t, \quad (8a)$$

$$\ddot{x}_2 + 2\mu_2 \dot{x}_2 + \omega_2^2 x_2 + \Lambda_4 x_1^2 + \Lambda_5 x_1 x_2 + \Lambda_6 x_2^2 = f_2 \cos \Omega t. \quad (8b)$$

The expressions of the damping terms μ_1 and μ_2 , the nonlinear coefficients Λ_k , and the modal forcing terms f_1 and f_2 are given in [8]. This last system (8a,b) is at the basis of the theoretical analysis of [8] since it is the canonical system to study the 2 : 1 internal resonance and its dynamical effects (nonlinear antiresonance and saturation phenomenon), as recalled in the following.

2.2 Typical response and saturation phenomenon

To illustrate the features of the 2 : 1 internal resonance, we present the solution of (8a,b) to the first order with $\omega_2 \approx 2\omega_1$ which reads [6] :

$$x_1(t) = a_1 \cos\left(\frac{\Omega}{2}t - \frac{\gamma_1 + \gamma_2}{2}\right), \quad x_2(t) = a_2 \cos(\Omega t - \gamma_2), \quad (9)$$

where a_1 and a_2 are the amplitudes, γ_2 is the phase angle of $x_2(t)$, and γ_1 represents the relative phase angle between $x_1(t)$ and $x_2(t)$. The closed-form expressions of the amplitudes and phase angles (obtained with a first-order multiple scale method, MSM). The typical response is illustrated in Figure 3. It shows the response of amplitudes a_1 and a_2 with respect to the detuning $\sigma_1 = \bar{\Omega} - \omega_2$ for different excitation levels. This typical response is done by neglecting the nonresonant terms (i.e., $\Lambda_1 = \Lambda_3 = \Lambda_5 = \Lambda_6 = 0$). One can observe three main features :

- Figure 3(a) shows that when the linear response enters an instability region (shaded in blue), energy transfer to the low-frequency mode occurs, leading to the activation of a_1 . Consequently, an antiresonance appears that replaces the primary resonance.
- Figure 3(b) focuses on the amplitude at the resonance frequency (a_1^* and a_2^*). It shows that after a threshold forcing, a_2^* becomes independent from the excitation level (i.e. saturation phenomenon) and a_1^* keeps increasing.
- Figure 3(c) shows that γ_1 is locked at $3\pi/2$ at the antiresonance frequency. This feature is important in further analysis.

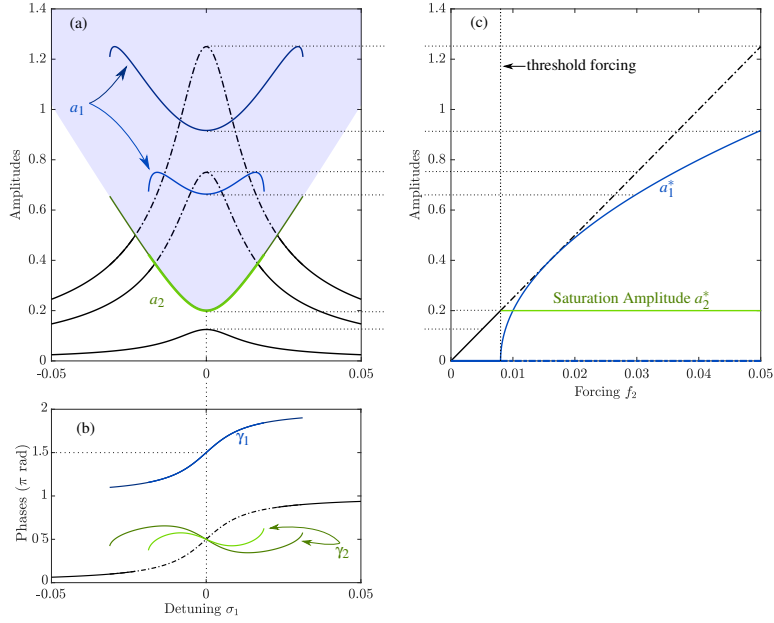


FIGURE 3 – Typical response of the amplitudes a_1 and a_2 and the phases γ_1 and γ_2 , stemming from the first order multiple solution of system (8a,b), for $\omega_2 = 2\omega_1$. The numerical values are $\Lambda_2 = \Lambda_4 = 0.1$, $\mu_1 = 0.005$, $\mu_2 = 0.01$. (a) and (b) show respectively the amplitude and phase response with respect to the detuning σ_1 for values of the forcing f_2 ($f_2 \in \{0.005; 0.03; 0.05\}$). (c) amplitude response at the resonance frequency ($\sigma_1 = 0$) with respect to the excitation level f_2 . In the plots, the linear responses of a_2 and γ_2 are plotted in black. The solid and the dashed-dotted lines denote respectively the stable and the unstable solutions.

To link the features shown in Figure 3 to the physical response, the displacement $\mathbf{u}(t)$ and the charge $Q(t)$ can be expressed, using (6), as :

$$\mathbf{u}(t) = \frac{\Phi_i}{\sqrt{m_i}} \left[\underbrace{-\varepsilon a_1 \cos\left(\frac{\Omega}{2}t - \frac{\gamma_1 + \gamma_2}{2}\right)}_{x_1(t)} + \underbrace{a_2 \cos(\Omega t - \gamma_2)}_{x_2(t)} \right], \quad (10a)$$

$$Q(t) = \frac{1}{\sqrt{L}} \left[\underbrace{a_1 \cos\left(\frac{\Omega}{2}t - \frac{\gamma_1 + \gamma_2}{2}\right)}_{x_1(t)} + \varepsilon \underbrace{a_2 \cos(\Omega t - \gamma_2)}_{x_2(t)} \right]. \quad (10b)$$

Consequently, $\mathbf{u}(t)$ and $Q(t)$ are mainly composed of two harmonics, at $\Omega/2$ (harmonic H1/2) and at Ω (harmonic H1). Because of the small value of ε , the leading harmonics in the response of $\mathbf{u}(t)$ and $Q(t)$ are, respectively, H1 and H1/2. Moreover, since there is a frequency splitting in the expression of $\mathbf{u}(t)$, the saturation phenomenon seen in the response of $x_2(t)$ is equally observed in the H1 harmonic response of the displacement.

2.3 Effect of the nonresonant terms and correction of the antiresonance

The first-order multiple scale solution shown in Figure 3 neglects the effects of the nonresonant terms. However, as shown in [8], one of those terms, namely Λ_1 , admits a very large value compared to the resonant terms Λ_2 and Λ_4 . This leads to an unusual and major effect that quantitatively modifies the ideal response of Figure 3. This is illustrated in Figure 4 in which a numerical solution of (2a,b), obtained with the continuation software Manlab [11], is shown. The modal parameters used to obtain the numerical solution are estimated experimentally and gathered in Table 1 which correspond to the cantilever beam structure shown in Figure 6, with the displacement $u(t)$ considered at the beam tip ($u(t) = q_i(t)$ with a mode shape scaled to 1). One can observe that the resonance frequency $\hat{\omega}_1$ (for $\beta = 0$) is slightly higher than the open circuit frequency $\hat{\omega}_1$ due to the PE coupling.

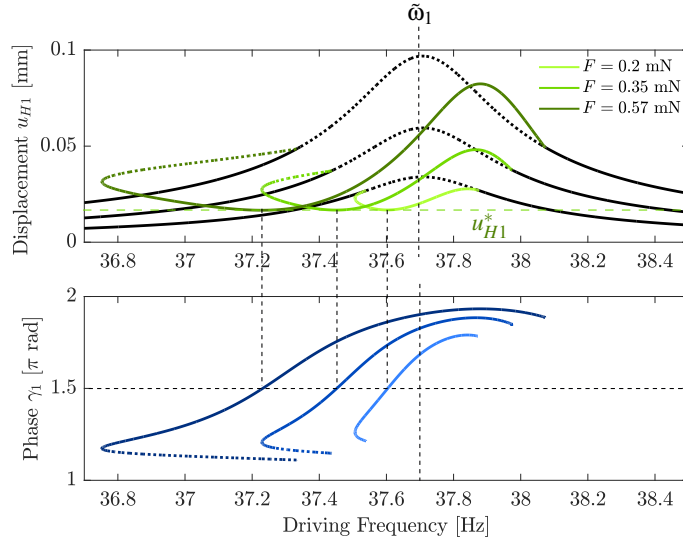


FIGURE 4 – Frequency response of the beam tip displacement first harmonic u_{H1} amplitude, the charge $Q_{H1/2}$ subharmonic and the phase γ_1 , obtained by solving system (2a,b) using Manlab for several excitation levels. The numerical values are $\beta = 0.012$, $r_i = 0.52$, and $\xi_e = 0.002$. The linear response is plotted in black. The solid and dotted lines denote, respectively, the stable and the unstable solutions.

By observing the physical response of the amplitudes corresponding to the H1 and H1/2 harmonics of the displacement and charge (u_{H1} and $Q_{H1/2}$), shown in Figure 4, and by comparison with the typical response illustrated in Figure 3, the effect of the nonresonant terms can be inferred [8] :

- the antiresonance shifts to low frequencies with increasing excitation level, violating the saturation phenomenon ;
- although the antiresonance is shifting, its amplitude remains constant at a saturation amplitude u_{H1}^* , which is the same as a_2^* analytically obtained with the MSM ;
- the phase angle γ_1 is kept locked at $3\pi/2$ at the antiresonance point ;

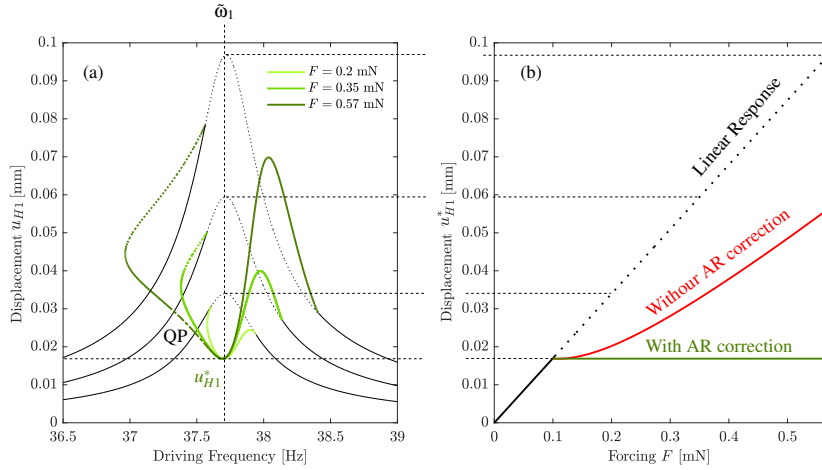


FIGURE 5 – (a) Frequency response of the first harmonic amplitude of the beam tip displacement u_{H1} , estimated by solving system (2a,b) using Manlab, for several excitation levels and with AR correction. (b) First harmonic amplitude of the beam tip displacement at the resonance frequency u_{H1}^* with respect to the excitation level, with and without AR correction. The plots are done for $\beta = 0.012$. The displacement linear response is plotted in black. The solid and dotted/dashed lines denote, respectively, the stable and unstable solutions. QP refers to a quasi-periodic response.

The main aim of this work is to exploit the saturation phenomenon, which is violated due to the effect of the nonresonant terms. To correct this, we proposed an antiresonance correction (AR correction)

TABLE 1 – Electro-mechanical modal parameters of the first bending mode of the cantilever beam (subscript $i = 1$).

| Parameters | $\tilde{\omega}_i/(2\pi)$ [Hz] | $\hat{\omega}_1/(2\pi)$ [Hz] | $\xi_1(\%)$ | k_1 | θ_1 [mN/V] | m_1 [g] | C_{p1} [nF] |
|------------|--------------------------------|------------------------------|-------------|-------|-------------------|-----------|---------------|
| Value | 36.6 | 37.51 | 0.5 | 0.20 | 0.8 | 8.8 | 32.45 |

technique, that consists in locking the antiresonance by choosing the proper value of the ratio r_i for each excitation level *to counter-balance* the shifting observed in Figure 4. As shown in detail in [8], this can be simulated by a numerical continuation of the system (2a,b) using Manlab, to obtain the amplitude of u_{H1} as a function of r_i for a certain excitation level and with a prescribed driving frequency equal to the resonance frequency shown in Figure 4 ($\tilde{\omega}_1 = 37.7$ Hz). Then, the value of r_i where u_{H1} achieves its minimum value is the required value to lock the antiresonance at the resonance frequency.

Following the AR correction, the response of u_{H1} shown in Figure 4 is replaced by the one shown in Figure 5(a) where it clearly shows that the antiresonance is locked at $\tilde{\omega}_1$. One can note the appearance of a quasi-periodic solution (QP) for $F = 0.57$ mN. Also, Figure 5(b) shows the amplitude of u_{H1}^* with respect to the excitation level, where one can observe that the proposed AR correction preserves the saturation phenomenon.

3 Experimental Analysis

3.1 Structure under test

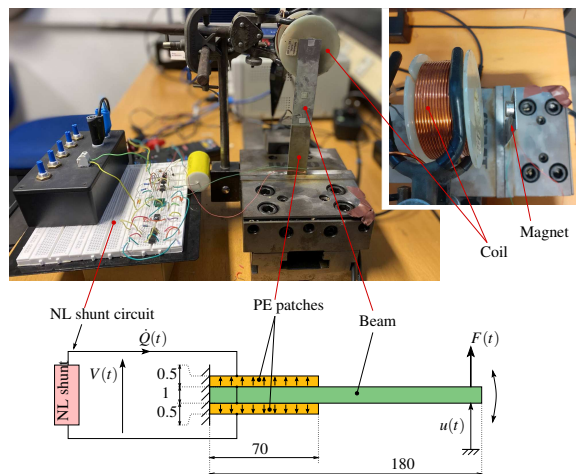


FIGURE 6 – Experimental setup. Dimensions are in mm. The width of the beam and PE patches is 30.5 mm.

The experimental tests were conducted on a cantilever beam with two PIC 151 piezoelectric (PE) patches symmetrically glued on the two faces of a stainless steel beam, as shown in Figure 6. The nonlinear shunt circuit is connected to the structure with the PE patches in series and with opposite polarizations to couple the electrical shunt circuit to the bending of the beam. A contactless electromagnetic actuator composed of a fixed coil and a magnet attached to the structure tip is used to generate an electromagnetic force by inducing a current in the coil.

3.2 Experimental results

The two main experimental quantities that have been measured are the beam tip velocity $v(t)$ and the PE patch voltage $V(t)$ using a laser vibrometer and a voltage probe, respectively. To validate the

energy transfer, only the amplitudes of the fundamental harmonic of the velocity (v_{H1}) and the first subharmonic amplitude of the voltage ($V_{H1/2}$) are estimated. To have the frequency response of the harmonics, a stepped sine measurement has been performed. Namely, a single harmonic sinusoidal signal with a certain frequency is amplified and sent to the coil. Then, using a demodulation procedure [9], v_{H1} and $V_{H1/2}$ are estimated from the time signals $v(t)$ and $V(t)$. This procedure is repeated for different excitation frequencies to have the desired frequency response. More details regarding the experimental protocol and the nonlinear shunt circuit can be found in [9].

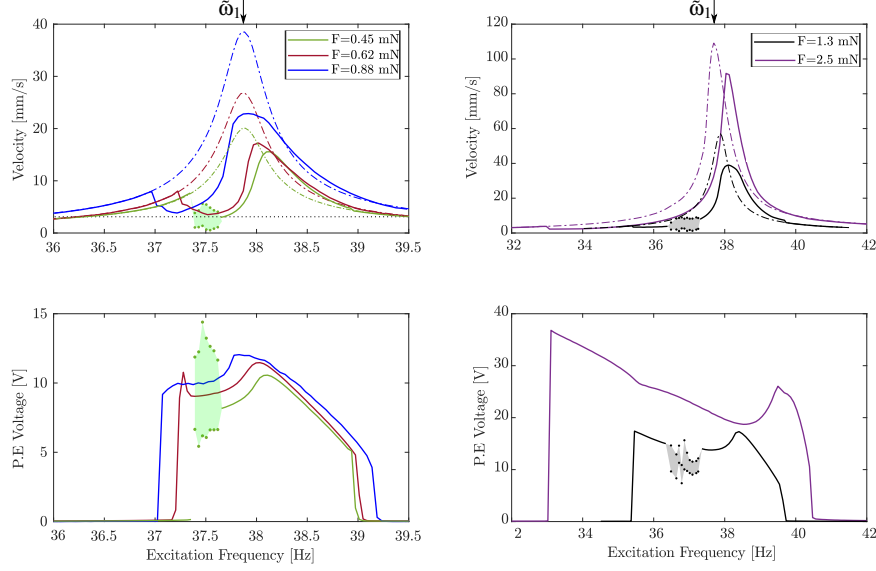


FIGURE 7 – Experimental results of v_{H1} (first row) and $V_{H1/2}$ (second row) for several excitation levels. Only the data for sweeping down the excitation frequency are shown in solid lines. The measurements are done for $\beta = 0.035$, $\xi_e = 0.002$, and $r_1 = 0.537$. The shaded regions depict the quasi-periodic regime.

The effect of the excitation level on the response is illustrated in Figure 7, where only downward frequency sweeps are shown. The ratio r_1 is also chosen to have $\omega_1/\omega_2 \simeq 0.5$ and activate the internal resonance to take into account the effect of the piezoelectric coupling. One can realize that increasing

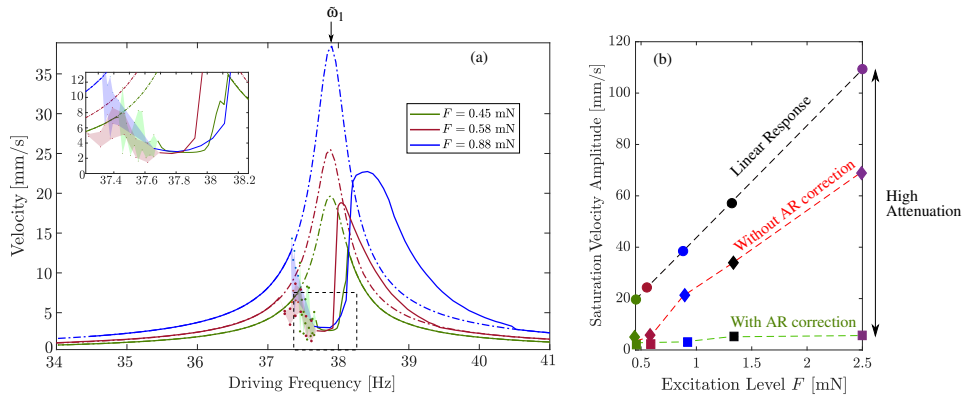


FIGURE 8 – (a) Experimental frequency response of v_{H1} for sweeping down the excitation frequency for several excitation levels with the AR correction. (b) Antiresonance saturation amplitude v_{H1}^* at the resonance frequency $\tilde{\omega}_1$ versus the excitation level plotted for three different cases : the linear response - \bullet -, with fixed $r_1 = 0.537$ - \blacklozenge -, and with the AR correction in - \blacksquare -. The curves are estimated for $\beta = 0.035$ and $\xi_e = 0.002$.

the excitation amplitude while keeping the other design parameters fixed leads to increased velocity and PE patch voltage amplitudes. Looking at the antiresonance, one can observe that its amplitude remains almost constant with the increase of the excitation level but shifts to lower frequencies as the excita-

tion level increases. This validates the numerical predictions in Figure 4, suggesting a violation of the saturation phenomenon at a fixed excitation frequency.

Our purpose is to preserve the saturation phenomenon to enhance the absorber’s efficiency. Because the antiresonance amplitude remains constant, it is sufficient to lock the antiresonance at the resonance frequency. Experimentally, the AR correction is performed using the preserved feature of $\gamma_1 = 3\pi/2$ at the antiresonance point. Namely, before performing the stepped sine measurements, a sinusoidal signal of frequency equal to the mechanical resonance frequency $\tilde{\omega}_1/(2\pi) = 37.75$ Hz is amplified to the desired excitation level and then fed to the coil. The required value of r_i , which is controlled by the inductance in the circuit, is the one that locks γ_1 at $3\pi/2$. To ensure the lockage value of γ_1 , the velocity $v(t)$ and the PE patch voltage $V(t)$ are visualized using an oscilloscope in an XY mode to obtain a Lissajous plot, which has a unique shape for $\gamma_1 = 3\pi/2$. The same process is repeated for each excitation level to have the required value of the inductance that locks the antiresonance at $\tilde{\omega}_1/(2\pi) = 37.75$ Hz. With the AR correction, the stepped sine measurements are performed again for different excitation levels, and the response of v_{H1} shown in Figure 7 is replaced by that shown in Figure 8 where the saturation is almost preserved with a high attenuation level at the highest excitation.

4 Conclusion

This abstract addresses a theoretical and experimental study for a new semi-passive nonlinear piezoelectric shunt absorber. This absorber is designed by intentionally adding a quadratic nonlinear voltage source in series with a resonant shunt circuit. This is done to activate the 2 :1 internal resonance and consequently obtain a nonlinear antiresonance in place of the primary resonance accompanied with an amplitude saturation. The main drawback of the designed absorber is the unexpected detuning of the shunt as a function of the amplitude, leading to the loss of the saturation phenomenon. This was manually corrected by a phase-locking of the PE voltage with the mechanical response of the structure. The experimental results validated the numerical prediction and showed a high attenuation level at higher excitation levels. An alternative way to preserve the saturation is to introduce an additional cubic nonlinear component to the shunt circuit, which will be shown in a future study.

Références

- [1] N. W. Hagood and A. Von Flotow. Damping of structural vibrations with piezoelectric materials and passive electrical networks. *Journal of Sound and Vibration*, 146(2) :243–268, 1991.
- [2] M. Berardengo, S. Manzoni, O. Thomas, and M. Vanali. Piezoelectric resonant shunt enhancement by negative capacitances : Optimisation, performance and resonance cancellation. *Journal of Intelligent Material Systems and Structures*, 29(12) :2581–2606, 2019.
- [3] A. F. Vakakis and O. Gendelman. Energy pumping in nonlinear mechanical oscillators : Part ii - resonance capture. *Journal of Applied Mechanics*, 68 :42–48, 2001.
- [4] B. Zhou, F. Thouverez, and D. Lenoir. Essentially nonlinear piezoelectric shunt circuits applied to mistuned bladed disks. *Journal of Sound and Vibration*, 333 :2520–2542, 2014.
- [5] T M. P. Silva, M. A. Clementino, C. De Marqui Jr., and A. Erturk. An experimentally validated piezoelectric nonlinear energy sink for wideband vibration attenuation. *Journal of Sound and Vibration*, 437 :68–78, 2018.
- [6] A. H. Nayfeh and D. T. Mook. *Nonlinear Oscillations*. John Wiley & Sons, inc., New-York, 1979.
- [7] P. F. Pai, B. Wen, A. S. Naser, and M. J. Schultz. Structural vibration control using pzt patches and non-linear phenomena. *Journal of Sound and Vibration*, 215(2) :273–296, 1998.
- [8] Z.A. Shami and C. Giraud-Audine and O. Thomas. A nonlinear piezoelectric shunt absorber with a 2 :1 internal resonance : theory. *Mechanical Systems and Signal Processing*, 2021. Under Review.
- [9] Z.A. Shami and C. Giraud-Audine and O. Thomas. A nonlinear piezoelectric shunt absorber with 2 :1 internal resonance : experimental proof of concept. *Smart Materials and Structures*, 2021. Under Review.
- [10] M. Berardengo, O. Thomas, C. Giraud-Audine, and S. Manzoni. Improved resistive shunt by means of negative capacitance : New circuit, performances and multi-mode control. *Smart Materials and Structures*, 25(7) :075033, July 2016.
- [11] L. Guillot, B. Cochelin, and C. Vergez. A Taylor series-based continuation method for solutions of dynamical systems. *Nonlinear Dynamics*, 98(4) :2827–2845, December 2019.